Paper:
David Kirubakaran, D., Ravi Dhas, C., Jain, S., Marchesi, L. & Pitchaimuthu, S. (2019). Jet nebulizer-spray coated CZTS film as Pt-free electrocatalyst in photoelectrocatalytic fuel cells. *Applied Surface Science, 463*, 994-1000.
http://dx.doi.org/10.1016/j.apsusc.2018.08.178

Jet nebulizer-spray coated CZTS film as Pt-free electrocatalyst in photoelectrocatalytic fuel cells

D. David Kirubakaran,[a] C. Ravi Dhas,[a] Sagar M. Jain,[b], Luis F. Marchesi,[c] Sudhagar Pitchaimuthu[b*]

a. PG & Research, Department of Physics, Bishop Heber College (Autonomous), Tiruchirappalli-620017, India

b. Multi-functional Photocatalyst and Coatings Group, SPECIFIC, Materials Research Center, College of Engineering, Swansea University (Bay Campus), Swansea SA1 8EN, Wales, United Kingdom.

c. UniversidadeTecnológica Federal do Paraná, Av. Monteiro Lobato s/n Km04, CEP 84016-210, Ponta Grossa - PR, Brazil

* Corresponding authors: S.Pitchaimuthu@swansea.ac.uk

Abstract

The copper zinc tin sulphide (CZTS) is a promising p-type earth abundant alloy that received profound attention as an electron driven dark catalyst in electrocatalytic reduction reactions. In particular, the photoelectrocatalysis based solar fuel cell encompass with inexpensive electrocatalyst (hydrogen evolution reaction) is anticipated to support to reduce the overall system cost. However, demonstrating CZTS as Pt-free counter electrode in photoelectrocatalytic fuel cells is scarce. Because, achieving high electronic conductivity, favourable (112) crystalline structure towards high electrocatalytic property through low cost vacuum-free technique is remains challenge. In this report, we demonstrate p-type CZTS film fabrication at different processing temperature (250, 300, and 350℃) using jet nebulizer spray (JNS) coating technique. The processing temperature play a key role on crystalline property, composition, and catalytic activity of CZTS. The x-ray diffraction and energy dispersive analysis results reveals that the CZTS film prepared 250℃ exhibit kesterite structure oriented in (112) direction. The electrocatalytic reduction property of as-synthesised CZTS electrodes in water reduction process is tested in aqueous 1 M NaOH solution. Among the different temperature processed films, CZTS prepared at 250℃ result high electrocatalytic reduction activity ~ -2.1 $mAcm^{-2}$ at -0.44 V vs Ag/AgCl. In addition, these film exhibits high electrical conductivity than that of other CZTS samples. Therefore, optimised CZTS 250℃ film is further examined in hydrogen peroxide (H_2O_2) reduction which result enhanced electrical current generation after adding the 1 M of hydrogen peroxide in PBS electrolyte based electrochemical cell. This encouraged to apply as Pt-free counter electrode in H_2O_2 electrolyte based photoelectrocatalytic fuel cells. The PEC cells encompass with TiO_2

nanowire photoelectrode, and CZTS-250˚C counter electrode showed feasible photocurrent generation compared to conventional Pt counter electrode. This proof-of-concept type Pt-free PEC cells leads to open new paths in implementing wide-range of semiconductor based electrocatalyst to support in development of low-cost photoelectrocatalytic fuel cells.

Keywords: CZTS; electrocatalyst; Jet nebulizer spray technique; water splitting; H_2O_2; photoelectrocatalytic fuel cell.

1. Introduction:

The photoelectrochemical (PEC) technique is a promising tool in energy generation [1] and offers flexible choice of electrolyte feed stock including sea water, industrial pollutant, and non-aqueous chemicals[2-5] . This facilitate to apply PEC in wide range of commodity valuable applications including cheap fuel generation (oxygen, and hydrogen), chemical synthesis, water treatment and value added to other applications[6]. Conventional PEC cell consists with photoanode, cathode and electrolyte is filled in between these components. Under light irradiation the photoelectrons generated from conduction band of photoanode will transfer to cathode component, which reduce the proton ions into hydrogen gas. In some cases, the photoelectrons involved in redox reaction on cathode component and flow of electrons in the external circuit generate electricity [7]. Based on the chemical reaction, the PEC cell will produce either electricity or fuel as output. Besides the advantages of PEC cell in energy generation, the overall cost of the system is challenging factor to bring it into market. Mainly, expensive platinum in PEC cathode component limits the practical implementation of PEC in energy generation applications.

In this context, developing less expensive semiconductor electrocatalyst to replace expensive Pt create significant economic impact in energy industries. The recent

advancements on Pt-free electrocatalyst in dye-sensitized solar [8, 9], using semiconductor based electrocatalyst is an inspiration to develop similar type of materials for PEC based fuel cells. Among the available Pt-free electrocatalyst materials, transition metal oxides, sulphides, nitrides and carbides showed promising electrocatalytic performance in DSSCs.[10-14] In addition, the quaternary semiconductor CZTS geared notable attention in DSSCs owing to less toxic, earth abundance,[15-18] and high hole concentration[19] of ~1.2×10^{15} to 3.1×10^{20} cm^{-3}. Digraskar et al [20] demonstrated the feasibility of CZTS electrocatalyst in powder form toward water reduction into hydrogen fuel. They showed exceptionally high current density ~130 mA/cm^2, at lower onset potential 300 mV v/s RHE with appreciable stability. However, transforming powder type electrocatalyst into film type electrode will be more technical challenge compared to direct film fabrication. Conversely, CZTS has been demonstrated as vital electrocatalyst in many reduction reactions such as oxygen reduction reaction for batteries[21], CO_2 reduction in to fuel [22], and triiodide reduction in DSSCs [23].

The CZTS films can be directly formed on substrates or deposited from the pre-synthesised nanocrystals. The pre-synthesised colloidal CZTS nanocrystals or inks were transformed onto conducting substrates by spin coating,[15, 16] or spray coating[17]. The hydrothermal/solvothermaldeposition,[18, 24]electrospun,[25, 26] spray coating,[27] electrodeposition,[28, 29] sputtering,[23] and pulsed laser deposition[24] methods have been used for direct deposition of CZTS onto substrates. Among these techniques, spray coating has been attracted much interest owing to its technical advantages to combine wet chemical, and physical process of nanomaterial synthesis [30, 31]. But the major challenge in spray coating process is inhomogeneous film formation with coagulated particle due to inadequate aerosol distribution from

conventional spray nozzle. It will affect the film integrity as well as electrocatalytic performance.[32] In this context, modified spray coater with jet-nebulizer nozzle will overcome the particle clogging issue at nozzle. Unlike conventional spray coating nozzle, the nebulizer will form cloud type aerosol facilitate uniform coating on the substrate [33-36]. This may anticipate to produce homogenous and highly reactive CZTS catalyst film.

In the present work, we fabricate CZTS film at different processing temperature using jet nebulizer spray (JNS) coating. The inter dependence of crystalline structure, and electrocatalytic property of as-synthesized CZTS films were examined and discussed in detail. The optimized electrode with good electrocatalytic activity will be integrating with photoabsorber in hydrogen peroxide based PEC fuel cells and their performance in electricity production is studied.

2. Experimental

2.a Jet nebulizer spray coated CZTS film: All the chemicals were received from Alfa Aesar India, and utilized without further purification. The typical precursor solutions are $CuCl_2$, $ZnCl_2$, $SnCl_2$, CH_4N_2S taken in the ratio of 2:1:1:8 and dissolved in 35 mL of distilled water and stirred constantly under room temperature for 30 min. Prior to deposition, the fluorinated tin oxide (FTO) substrates were cleaned with methanol, acetone and distilled water under ultrasonic bath. The resultant precursor solution was filtered to remove the residual components remain undissolved. The filtered precursor solution was taken in the pocket size nebulizer as demonstrated in our previous work [34] and spraying was carried out on the FTO substrate for 5 minutes. The distance between the substrate and sprayer nozzle is 10 cm. The aerosol generation at nebulizer container was transported by a carrier gas with constant pressure 0.2 kg/cm^2 on the

FTO substrate at spray rate of 0.75 ml/min. The substrate temperature of 250 °C was applied through hot plate as is shown in Scheme 1. During the deposition, the transported aerosol underwent decomposition reaction on the substrate surface and produce CZTS film. The schematic illustration of JNS coating set up is as shown in Scheme 1.

***2.b TiO_2 photoanode fabrication*:** The TiO_2 nanowire array onto FTO substrate is prepared using zinic oxide sacrificial template as is reported by Rodenaset al.[37] The thickness of the resultant film is approximately 1 micron.

2.c Characterization: The crystal structure of the as-deposited CZTS film was studied with X-ray diffractometer (Rigaku Denki Japan) using CuKα radiation. The surface morphology of CZTS was characterized using a field emission scanning electron microscope (FE-SEM, JSM 7600F, JEOL, Tokyo, Japan). The optical absorption of different temperature processed CZTS films is recorded using JASCO spectrophotometer.

2.c Electrochemical characterization: The electrochemical reduction and oxidation activity of CZTS films were studied through cyclic voltammetry (CV) analysis. The CV experiments were carried out using conventional three electrodes electrochemical cell. The commercial platinum wire is used as cathode and as-deposited CZTS film is applied as anode electrode. The Ag/AgCl electrode is used as reference electrode. The aqueous 1 M NaOH solution is used as electrolyte. To evaluate electrocatalytic reduction of H_2O_2 the optimized CZTS electrode was tested in 0.1 M phosphate buffered saline (PBS)(Sigma Aldrich, pH=7.1) solution in the presence and absence of 0.2 M H_2O_2.

2.d Photoelectrochemical fuel cell measurements: The TiO_2 nanowire was grown on FTO substrate using previously grown ZnO nanowire template as explained by

Rodenaset al.[38] The TiO_2 NW is applied as photoanode and optimized CZTS film is utilised as cathode. The Ag/AgCl electrode is used as reference electrode. The photocurrent measurements were recorded using a solar simulator with a 300 W xenon arc-lamp (Asahi Spectra- HAL 320). The light intensity ($100mWcm^{-2}$) was calibrated using a silicon photodiode. 0.2 M of hydrogen peroxide (Sigma Aldrich) was dispersed in 0.1 M PBS and was used as electrolyte for PEC measurements.

3. Results and discussion

3.a Structural analysis: The crystalline structure JNS coated CZTS thin films at different substrate temperatures (250, 300 and 350℃) were examined by x-ray diffractrometer (XRD). The results were summarized in **Figure 1a**. From **Figure 1a**, significant crystalline peaks were observed at 28.5˚, 47.3˚ and 56.2˚ are corresponding to (112), (220), and (312) crystalline planes of CZTS. These peaks were matched with kesterite tetragonal structure (JCPDS – 26-0575). The crystalline growth of CZTS by JNS spray coating rely on surface mobility of the atomic species on the substrate and intake metal precursor composition, which further control by substrate temperature. For instance, the CZTS coating at higher temperature (350℃) results high crystalline intensity peak along (112) c-axis ensure the temperature effect on crystal growth. The plausible reason for predominant crystal growth along (112) plane may due to the Cu enriched defect sites [7] and is in line with previous reports on spray coating [1,2,5] as well as other techniques [4,6]. The average crystalline size of CZTS films found to be increased from 24 nm to 57 nm by increasing processing temperature from 250 to 350℃. We experienced that the CZTS films were feel-off from the substrate while prepared below 250℃. Therefore, a minimum thermal energy is required for good CZTS film formation.

The degree of preferred orientation of the different crystalline planes at different processing temperatures were analysed through evaluating texture coefficient (TC) using the Harris analysis [39]

$$T_c = \frac{I_0(h_i k_i l_i)}{I_s(h_i k_i l_i)} \left(\frac{1}{N} \sum_{i=1} \frac{I_0(h_i k_i l_i)}{I_s(h_i k_i l_i)} \right)^{-1} \quad (1)$$

where h, k, and l are the Miller indices; $TC_{(hkl)}$ is the texture coefficient value of specific (hkl) planes; $I_{(hkl)}$ is the measured peak intensity; and ΣI(hkl) is the summation of the intensities for the (112), (220) and (312) peaks of the CZTS films.

The estimated TC values for different crystalline plane were presented in **Figure 1 (b)**. Compared to other crystalline phases of (220) and (312) the TC values are showed significant variation at (112) direction and CZTS-350℃ sample results higher TC=2.13 than that of other samples. This higher value of the TC corresponds to increase in planar density along (112) crystal plane [40, 41]. Here the TC variation with processing temperature dependence with several reasons including solvent evaporation rate and stability of material constituents during spray process. In literature, (112) crystalline phase are responsible for reactive sites in catalysis reaction as well as photo-absorber [42] applications. However, to synthesis highly selective (112) crystalline plane based CTZS is critical and remains challenge. The previous reports on (112) crystalline plane based CZTS films are selectively synthesised either of the coating routes such as the sacrificial templates, probing substrate temperature [42-44] or the sulfurization process[45]. The present work show that the substrate temperature can facilitate crystalline CZTS growth which favours highly selective (112) plane. It is worth to mention that achieving highly oriented (112) crystalline plane through JNS technique without assisting any binder additives and relatively less substrate temperature compare to conventional spray coating technique endorse their technical merit.[46, 47]

Further, crystalline phase of CZTS is studied by measuring the Raman spectra (**Figure 2**). The observed broad Raman peak at 322 cm^{-1} indicates the kesterite CZTS structure.[44, 48] A small shift in Raman peak position is often observed in due to difference in preparation technique and composition.[48] The intensity of Raman peak at 322 cm^{-1} slightly increased with temperature treatment.

Figure 3(a-c) shows the surface morphology of the CZTS film at 1-micron scale prepared at different temperatures. In CZTS-250 sample, the film surface seems to be compact packing of nanoscale crystallites (**Figure 3a**). The rugosity of the film surface might be related to the spray coating at low substrate temperature.[46] Further increasing processing temperature from 250 to 300℃ (**Figure 3b**) induce CZTS inter grain diffusion and result agglomeration. Above this processing temperature homogenous film growth turn into non-homogenous surface due to large anisotropy crystals formation (**Figure 3c)**. The elemental mapping analysis on CZTS-250˚C sample (**Figure 3d**) implies Cu, Zn, Sn and S ensure CZTS alloy formation.

The optical absorption properties of CZTS films were studied using Kulbelka-Munk relation. The resultant optical absorption results of all CZTS samples were summarised in **Figure 4 (a-c)**. Through extrapolation plot in fundamental absorption edge to X axis corresponding band gap energy values were obtained. From **Figure 4 (a-c)**, the band gap energy of CZTS is gradually decreased from 1.26 to 1.13 eV by increasing processing temperature. In practical, processing temperature of spray coating facilitate the crystal growth and thus reduce the band gap energy [49]. However, band gap energy of CZTS films from previous reports showed in between 1.3 – 1.8 eV[50, 51]. This indicates that the CZTS prepared at 250℃ using JNS technique is closer to stoichiometry. At high temperature either any one of components in CZTS may evaporate from the film which reduce the band gap energy.

The electron conductivity of electrode is an indispensable parameter to support high catalysis reaction. The electrical conductivity property of CZTS samples were studied through four probe analysis. The Log ρ vs 1000/T plot (**Figure 5**) is derived using conductivity results. From **Figure 5**, it clearly demonstrates that CZTS-250℃ showed high conductivity than other samples. It evinces that increasing processing temperature above 250℃ affect the conductivity of the film. Further we estimated carrier concentration (N_a) of the films from Figure 5. The CZTS 250℃ film results high value of N_a = 2.6 x 10^{16} cm^3. In the case of CZTS 300℃ and CZTS 350℃ samples showed N_a = 2.1 x 10^{16} cm^3 and 1.5 x 10^{16} cm^3, respectively. As is discussed above, one of the CZTS components may evaporate from the film will affect the carrier concentration of the films and thus affect the overall conductivity of the film. This is in line with previous reports [19] on high photovoltaic performance CZTS thin films in the order of 10^{15} to 10^{20} cm^{-3}. This strongly advocated that the JNScoated CZTS have excellent electronic conductivity which facilitates the electron carrier transport from electrode surface to catalytic reaction sites.

3.b Electrocatalytic property and hydrogen peroxide reduction:

Electrochemical water splitting into hydrogen and oxygen is one of the promising routes in low cost fuel generation.[52, 53] The proton reduction at cathode using electron carriers is a key process in hydrogen fuel generation;

$$4H^+ + 4e^- \Leftrightarrow 2H_2 (E^0{}_{red} = +0.000 V vs. NHE) \qquad (2)$$

In order to evaluate the capability of CZTS films in electrocatalytic water reduction reaction the cyclic voltomogram is recorded in aqueous 1 M NaOH (**Figure 6**). From **Figure 6**, the negative potential region indicates the water reduction process at CZTS electrode, and positive potential region corresponds to water oxidation process at

CZTS. In this work, our focus mainly on water reduction process rather water oxidation. In this view point, the CZTS-250℃ films showed high current density at ~ -2.1 $mAcm^{-2}$ at -0.44 V vs Ag/AgCl than other samples. This implies that CZTS 250℃ has high catalytic property towards water reduction. The observed high electrical conductivity of CZTS-250℃ from **Figure 5** can bring effective catalytic property to this sample.

Recently, electrocatalytic reduction of hydrogen peroxide (H_2O_2) also recognised as an alternative route to chemical energy storage compared to popularly practices in hydrogen and methanol based fuel cell.[54-56] Unlike hydrogen fuel cell, H_2O_2 fuel cells can operate in flexible environmental conditions, and does not require dioxygen environment, such as outer space and underwater conditions without membranes.[55] Moreover, production of H_2O_2 is industrially viable and can be applied as oxidant candidate in fuel cells instead of O_2 and it can substantially increase the theoretical voltage of fuel cells and thus improve cell performance.[55] Significant research has been proposed in direct electrocatalytic decomposition of H_2O_2 on the cathode and anode in a fuel cell. Recently, wide range of cathode materials such as metal, metallo-organic, enzyamatic are proposed in direct electrochemical decomposition of H_2O_2 process.[57-62] Despite of their performance, chemical interaction between H_2O_2 and catalyst surface is often challenge in direct electrocatalytic reduction process.

Therefore, we first analyse compatibility of CZTS electrode in reduction of H_2O_2 as it is shown in **Figure 7a**. For this experiment, we choose optimised CZTS-250℃ film as it possesses high catalytic property in water reduction reaction (**Figure 6**). Under applied potential, H_2O_2 will be oxidised into oxygen gas at Pt anode;[63]

$$H_2O_2 \rightarrow O_2 + 2H^+ + 2e^- \quad (3)$$

This reaction requires application of 0.69 V (NHE). Conversely, the two electrons from the anode will transport to CZTS cathode and it reduces H_2O_2 into H_2O;

$$H_2O_2 + 2H^+ + 2e^- \rightarrow 2H_2O \quad (4)$$

Figure 7b shows the CV plot of CZTS electrode at PBS electrolyte in the presence and absence of H_2O_2 (three electrode electrochemical configuration). The electrical current generation from electrochemical cell is drastically enhanced at -0.6 V vs Ag/AgCl after adding 1M of H_2O_2. This is attributed to the oxidative electrons generated from electrocatalytic oxidation of H_2O_2process at Pt surface and is transported to the circuit thus enhancing the electricity production in the charge collector.[64] The electrons collected at the Pt anode will be further transported to CZTS cathode surface that reduces the H_2O_2 into H_2O as explained in Eq. (2). This implies *that j-Neb* spray coated CZTS film can demonstrate the H_2O_2 reduction reaction at smaller potential compared to the metal cathodes requiring 1.77 V vs NHE.

3.d Membrane-free, hydrogen peroxide based photoelectrochemical fuel cell:

The photoelectrochemical (PEC) oxidation is a powerful tool in organic molecule decomposition. For instance, light driven titanium dioxide (TiO_2) photoelectrocatalyst can oxidise the target organic molecules at smaller applied voltage compared to electrocatalyst.[65] Also, the expensive Pt-anode can be managed by replacing low cost, light driven TiO_2 electrode. Recently, Dong and co-workers [66] demonstrated the PEC based H_2O_2 fuel cell using TiO_2 nanotube photoanode and Prussian Blue cathode.[66] Under UV light irradiation photoholes generated at valence band of TiO_2 NW will oxidize the H_2O_2 into oxygen. **Figure 8a** illustrates similar configuration of membrane-free H_2O_2 fuel cell modified with CZTS cathode and TiO_2 nanowire photoanode.

The photoelectrochemical measurements were carried out in the presence or absence of PBS electrolyte. The results are presented in **Figure 8b**. Photocurrent generation under light illumination is strikingly higher than that of dark condition explain the water oxidation process at TiO_2 photoanode lead by photoholes. Further, the photocurrent generation is markedly enhanced after adding the H_2O_2 in the electrolyte. The similar trend was observed in our previous report on photoelectrochemical glucose oxidation enhanced photocurrent generation.[67] Compared to Pt counter electrode (dotted line in **Figure 8b**), the CZTS cathode showed feasible current density in neutral pH condition (PBS electrolyte). Though two semiconductors TiO_2 and CZTS involved in PEC cells, the light driven catalysis process is only occurred at TiO_2 nanowire. Because optical band gap energy of CZTS-250ͦ sample showed 1.26 eV (**Figure 4a),** which lies in the visible light wavelength region. Therefore, under UV light irradiation CZTS does not produce photoelectroatalytic contribution like TiO_2. Further, introducing visible light driven photoanode (WO_3/$BiVO_4$) instead of TiO_2 in associate with JNS spray coated dark CZTS catalyst will be a futuristic fuel cell component in membrane-free solar light driven H_2O_2 fuel cell applications. Importantly, the feasibility of CZTS electrode has to be tested in acetic conditions (pH=1).

From the above discussion, though the JNS coated CZTS displayed reasonable performance in electrocatalytic reactions of H_2O_2 into H_2O yet their catalytic performance has to be improved. In particular, processing temperature dependence catalytic activity, long term durability at different electrolyte, pH environment will be necessitating for achieve industrial deployment.

4. Conclusions

In conclusion, aero-sol controlled CZTS film has been fabricated through low cost, nebulizer assisted spray coating technique. The as-deposited CZTS film prepared at 250°C processing temperature exhibits kesterite crystallite structure. Under identical experimental conditions, the CZTS films showed reasonable electrocatalytic performance in H_2O_2 reduction reactions, which encourages its implementation as Pt-free electrocatalyst in solar fuel cells. These results encourage application of the aero-sol controlled spray coated CZTS film as the low cost, earth abundance electrocatalyst, where reduction reaction takes a key role in energy conversion and energy storage systems.

Acknowledgement

The lead author S.P acknowledges Welsh Government and European Regional Development Fund (ERDF) for partial support of this project through Sêr Cymru II-Rising Star Fellowship program (80761-SU-102 (West)). In addition, this work was partially supported by the University Grants Commission, New Delhi, India [F.No. 42-903/ 2013(SR)] under Major Research Project Scheme (MRP).

References

[1] A. Fujishima, K. Honda, Electrochemical Photolysis of Water at a Semiconductor Electrode, Nature, 238 (1972) 37.

[2] Y. Li, R. Wang, H. Li, X. Wei, J. Feng, K. Liu, Y. Dang, A. Zhou, Efficient and Stable Photoelectrochemical Seawater Splitting with TiO2@g-C3N4 Nanorod Arrays Decorated by Co-Pi, The Journal of Physical Chemistry C, 119 (2015) 20283-20292.

[3] K. Mase, M. Yoneda, Y. Yamada, S. Fukuzumi, Seawater usable for production and consumption of hydrogen peroxide as a solar fuel, Nature Communications, 7 (2016) 11470.

[4] C. Haisch, J. Schneider, M. Fleisch, H. Gutzmann, T. Klassen, D.W. Bahnemann, Cold sprayed WO3 and TiO2 electrodes for photoelectrochemical water and methanol oxidation in renewable energy applications, Dalton Transactions, 46 (2017) 12811-12823.

[5] L. Sun, Y. Wang, F. Raziq, Y. Qu, L. Bai, L. Jing, Enhanced photoelectrochemical activities for water oxidation and phenol degradation on WO(3) nanoplates by transferring electrons and trapping holes, Scientific Reports, 7 (2017) 1303.

[6] V. Augugliaro, G. Camera-Roda, V. Loddo, G. Palmisano, L. Palmisano, J. Soria, S. Yurdakal, Heterogeneous Photocatalysis and Photoelectrocatalysis: From Unselective Abatement of Noxious Species to Selective Production of High-Value Chemicals, The Journal of Physical Chemistry Letters, 6 (2015) 1968-1981.

[7] S.-J. Yuan, G.-P. Sheng, W.-W. Li, Z.-Q. Lin, R.J. Zeng, Z.-H. Tong, H.-Q. Yu, Degradation of Organic Pollutants in a Photoelectrocatalytic System Enhanced by a Microbial Fuel Cell, Environmental Science & Technology, 44 (2010) 5575-5580.

[8] M. Wu, X. Lin, Y. Wang, L. Wang, W. Guo, D. Qi, X. Peng, A. Hagfeldt, M. Grätzel, T. Ma, Economical Pt-Free Catalysts for Counter Electrodes of Dye-Sensitized Solar Cells, Journal of the American Chemical Society, 134 (2012) 3419-3428.

[9] J. Briscoe, S. Dunn, The Future of Using Earth-Abundant Elements in Counter Electrodes for Dye-Sensitized Solar Cells, Advanced Materials, 28 (2016) 3802-3813.

[10] J. Guo, S. Liang, Y. Shi, C. Hao, X. Wang, T. Ma, Transition metal selenides as efficient counter-electrode materials for dye-sensitized solar cells, Physical Chemistry Chemical Physics, 17 (2015) 28985-28992.

[11] H.K. Mulmudi, S.K. Batabyal, M. Rao, R.R. Prabhakar, N. Mathews, Y.M. Lam, S.G. Mhaisalkar, Solution processed transition metal sulfides: application as counter

electrodes in dye sensitized solar cells (DSCs), Physical Chemistry Chemical Physics, 13 (2011) 19307-19309.

[12] Q. Lu, Y. Yu, Q. Ma, B. Chen, H. Zhang, 2D Transition-Metal-Dichalcogenide-Nanosheet-Based Composites for Photocatalytic and Electrocatalytic Hydrogen Evolution Reactions, Advanced Materials, 28 (2016) 1917-1933.

[13] S. Das, P. Sudhagar, S. Nagarajan, E. Ito, S.Y. Lee, Y.S. Kang, W. Choi, Synthesis of graphene-CoS electro-catalytic electrodes for dye sensitized solar cells, Carbon, 50 (2012) 4815-4821.

[14] J. Soo Kang, M.-A. Park, J.-Y. Kim, S. Ha Park, D. Young Chung, S.-H. Yu, J. Kim, J. Park, J.-W. Choi, K. Jae Lee, J. Jeong, M. Jae Ko, K.-S. Ahn, Y.-E. Sung, Reactively sputtered nickel nitride as electrocatalytic counter electrode for dye- and quantum dot-sensitized solar cells, Scientific Reports, 5 (2015) 10450.

[15] S. Chen, J. Tao, H. Tao, Y. Shen, L. Zhu, J. Jiang, X. Zeng, T. Wang, Fabrication of low cost kesterite Cu2ZnSnS4 (CZTS) thin films as counter-electrode for dye sensitised solar cells (DSSCs), Materials Technology, 30 (2015) 306-312.

[16] X. Xin, M. He, W. Han, J. Jung, Z. Lin, Low-Cost Copper Zinc Tin Sulfide Counter Electrodes for High-Efficiency Dye-Sensitized Solar Cells, Angewandte Chemie International Edition, 50 (2011) 11739-11742.

[17] X. Zhang, X. Wu, A. Centeno, M.P. Ryan, N.M. Alford, D.J. Riley, F. Xie, Significant Broadband Photocurrent Enhancement by Au-CZTS Core-Shell Nanostructured Photocathodes, Scientific Reports, 6 (2016) 23364.

[18] S. Chen, A. Xu, J. Tao, H. Tao, Y. Shen, L. Zhu, J. Jiang, T. Wang, L. Pan, In-Situ and Green Method To Prepare Pt-Free Cu2ZnSnS4 (CZTS) Counter Electrodes for Efficient and Low Cost Dye-Sensitized Solar Cells, ACS Sustainable Chemistry & Engineering, 3 (2015) 2652-2659.

[19] S. Chen, A. Walsh, X.-G. Gong, S.-H. Wei, Classification of Lattice Defects in the Kesterite Cu2ZnSnS4 and Cu2ZnSnSe4 Earth-Abundant Solar Cell Absorbers, Advanced Materials, 25 (2013) 1522-1539.

[20] R.V. Digraskar, B.B. Mulik, P.S. Walke, A.V. Ghule, B.R. Sathe, Enhanced Hydrogen Evolution Reactions on Nanostructured Cu2ZnSnS4 (CZTS) Electrocatalyst, Applied Surface Science, 412 (2017) 475-481.

[21] X. Yu, D. Wang, J. Liu, Z. Luo, R. Du, L.-M. Liu, G. Zhang, Y. Zhang, A. Cabot, Cu2ZnSnS4 Nanocrystals as Highly Active and Stable Electrocatalysts for the Oxygen Reduction Reaction, The Journal of Physical Chemistry C, 120 (2016) 24265-24270.

[22] T. Arai, S. Tajima, S. Sato, K. Uemura, T. Morikawa, T. Kajino, Selective CO2 conversion to formate in water using a CZTS photocathode modified with a ruthenium complex polymer, Chemical Communications, 47 (2011) 12664-12666.

[23] M.-S. Fan, J.-H. Chen, C.-T. Li, K.-W. Cheng, K.-C. Ho, Copper zinc tin sulfide as a catalytic material for counter electrodes in dye-sensitized solar cells, Journal of Materials Chemistry A, 3 (2015) 562-569.

[24] S. Wozny, K. Wang, W. Zhou, Cu2ZnSnS4 nanoplate arrays synthesized by pulsed laser deposition with high catalytic activity as counter electrodes for dye-sensitized solar cell applications, Journal of Materials Chemistry A, 1 (2013) 15517-15523.

[25] S.S. Mali, P.S. Patil, C.K. Hong, Low-Cost Electrospun Highly Crystalline Kesterite Cu2ZnSnS4 Nanofiber Counter Electrodes for Efficient Dye-Sensitized Solar Cells, ACS Applied Materials & Interfaces, 6 (2014) 1688-1696.

[26] M.K. Gonce, M. Dogru, E. Aslan, F. Ozel, I.H. Patir, M. Kus, M. Ersoz, Photocatalytic hydrogen evolution based on Cu2ZnSnS4, Cu2ZnSnSe4 and Cu2ZnSnSe4-xSx nanofibers, RSC Advances, 5 (2015) 94025-94028.

[27] S.K. Swami, N. Chaturvedi, A. Kumar, N. Chander, V. Dutta, D.K. Kumar, A. Ivaturi, S. Senthilarasu, H.M. Upadhyaya, Spray deposited copper zinc tin sulphide (Cu2ZnSnS4) film as a counter electrode in dye sensitized solar cells, Physical Chemistry Chemical Physics, 16 (2014) 23993-23999.

[28] H. Chen, Q. Ye, X. He, J. Ding, Y. Zhang, J. Han, J. Liu, C. Liao, J. Mei, W. Lau, Electrodeposited CZTS solar cells from Reline electrolyte, Green Chemistry, 16 (2014) 3841-3845.

[29] V.G. Rajeshmon, C.S. Kartha, K.P. Vijayakumar, C. Sanjeeviraja, T. Abe, Y. Kashiwaba, Role of precursor solution in controlling the opto-electronic properties of spray pyrolysed Cu2ZnSnS4 thin films, Solar Energy, 85 (2011) 249-255.

[30] D. Vak, S.-S. Kim, J. Jo, S.-H. Oh, S.-I. Na, J. Kim, D.-Y. Kim, Fabrication of organic bulk heterojunction solar cells by a spray deposition method for low-cost power generation, Applied Physics Letters, 91 (2007) 081102.

[31] A. Abdellah, B. Fabel, P. Lugli, G. Scarpa, Spray deposition of organic semiconducting thin-films: Towards the fabrication of arbitrary shaped organic electronic devices, Organic Electronics, 11 (2010) 1031-1038.

[32] M. Shao, S. Das, K. Xiao, J. Chen, J.K. Keum, I.N. Ivanov, G. Gu, W. Durant, D. Li, D.B. Geohegan, High-performance organic field-effect transistors with dielectric and active layers printed sequentially by ultrasonic spraying, Journal of Materials Chemistry C, 1 (2013) 4384-4390.

[33] S.S. Latthe, P. Sudhagar, C. Ravidhas, A. Jennifer Christy, D. David Kirubakaran, R. Venkatesh, A. Devadoss, C. Terashima, K. Nakata, A. Fujishima, Self-cleaning and superhydrophobic CuO coating by jet-nebulizer spray pyrolysis technique, CrystEngComm, 17 (2015) 2624-2628.

[34] C. Ravidhas, B. Anitha, A. Moses Ezhil Raj, K. Ravichandran, T.C. Sabari Girisun, K. Mahalakshmi, K. Saravanakumar, C. Sanjeeviraja, Effect of nitrogen doped titanium dioxide (N-TiO2) thin films by jet nebulizer spray technique suitable for photoconductive study, Journal of Materials Science: Materials in Electronics, 26 (2015) 3573-3582.

[35] C. Ravidhas, B. Anitha, D. Arivukarasan, R. Venkatesh, A.J. Christy, K. Jothivenkatachalam, A. Nithya, A. Moses Ezhil Raj, K. Ravichandran, C. Sanjeeviraja, Tunable morphology with selective faceted growth of visible light active TiO2 thin films by facile hydrothermal method: structural, optical and photocatalytic properties, Journal of Materials Science: Materials in Electronics, 27 (2016) 5020-5032.

[36] C. Ravi Dhas, R. Venkatesh, D. David Kirubakaran, J. Princy Merlin, B. Subramanian, A. Moses Ezhil Raj, Electrochemical sensing of glucose and photocatalytic performance of porous Co3O4 films by nebulizer spray technique, Materials Chemistry and Physics, 186 (2017) 561-573.

[37] R. Pau, S. Taesup, S. Pitchaimuthu, M. Gabriela, H. Hyungkyu, B.B. Laura, G. Sixto, F.S. Francisco, M.S. Ivan, B. Juan, P. Ungyu, K.Y. Soo, Quantum Dot Based Heterostructures for Unassisted Photoelectrochemical Hydrogen Generation, Advanced Energy Materials, 3 (2013) 176-182.

[38] P. Rodenas, T. Song, P. Sudhagar, G. Marzari, H. Han, L. Badia-Bou, S. Gimenez, F. Fabregat-Santiago, I. Mora-Sero, J. Bisquert, U. Paik, Y.S. Kang, Quantum Dot Based Heterostructures for Unassisted Photoelectrochemical Hydrogen Generation, Advanced Energy Materials, 3 (2013) 176-182.

[39] G.B. Harris, X. Quantitative measurement of preferred orientation in rolled uranium bars, The London, Edinburgh, and Dublin Philosophical Magazine and Journal of Science, 43 (1952) 113-123.

[40] B.D. Cullity, S.R. Stock, Elements of X-Ray Diffraction (3rd Edition), Prentice Hall, 2001.

[41] M. Kumar, A. Kumar, A.C. Abhyankar, Influence of Texture Coefficient on Surface Morphology and Sensing Properties of W-Doped Nanocrystalline Tin Oxide Thin Films, ACS Applied Materials & Interfaces, 7 (2015) 3571-3580.

[42] M.P. Suryawanshi, G.L. Agawane, S.M. Bhosale, S.W. Shin, P.S. Patil, J.H. Kim, A.V. Moholkar, CZTS based thin film solar cells: a status review, Materials Technology, 28 (2013) 98-109.

[43] K. Oishi, G. Saito, K. Ebina, M. Nagahashi, K. Jimbo, W.S. Maw, H. Katagiri, M. Yamazaki, H. Araki, A. Takeuchi, Growth of Cu2ZnSnS4 thin films on Si (100) substrates by multisource evaporation, Thin Solid Films, 517 (2008) 1449-1452.

[44] W. Li, K. Jiang, J. Zhang, X. Chen, Z. Hu, S. Chen, L. Sun, J. Chu, Temperature dependence of phonon modes, dielectric functions, and interband electronic transitions in Cu2ZnSnS4 semiconductor films, Physical Chemistry Chemical Physics, 14 (2012) 9936-9941.

[45] H.-W. Tsai, C.-W. Chen, S.R. Thomas, C.-H. Hsu, W.-C. Tsai, Y.-Z. Chen, Y.-C. Wang, Z.M. Wang, H.-F. Hong, Y.-L. Chueh, Facile Growth of Cu2ZnSnS4 Thin-Film by One-Step Pulsed Hybrid Electrophoretic and Electroplating Deposition, Scientific Reports, 6 (2016) 19102.

[46] M. Valdés, G. Santoro, M. Vázquez, Spray deposition of Cu2ZnSnS4 thin films, Journal of Alloys and Compounds, 585 (2014) 776-782.

[47] M.A. Majeed Khan, S. Kumar, M. Alhoshan, A.S. Al Dwayyan, Spray pyrolysed Cu2ZnSnS4 absorbing layer: A potential candidate for photovoltaic applications, Optics & Laser Technology, 49 (2013) 196-201.

[48] Z. Li, A.L.K. Lui, K.H. Lam, L. Xi, Y.M. Lam, Phase-Selective Synthesis of Cu2ZnSnS4 Nanocrystals using Different Sulfur Precursors, Inorganic Chemistry, 53 (2014) 10874-10880.

[49] P.K. Sarswat, M.L. Free, A study of energy band gap versus temperature for Cu2ZnSnS4 thin films, Physica B: Condensed Matter, 407 (2012) 108-111.

[50] T.K. Chaudhuri, D. Tiwari, Earth-abundant non-toxic Cu2ZnSnS4 thin films by direct liquid coating from metal–thiourea precursor solution, Solar Energy Materials and Solar Cells, 101 (2012) 46-50.

[51] N.S. Arul, D.Y. Yun, D.U. Lee, T.W. Kim, Strong quantum confinement effects in kesterite Cu2ZnSnS4 nanospheres for organic optoelectronic cells, Nanoscale, 5 (2013) 11940-11943.

[52] J. Luo, J.-H. Im, M.T. Mayer, M. Schreier, M.K. Nazeeruddin, N.-G. Park, S.D. Tilley, H.J. Fan, M. Grätzel, Water photolysis at 12.3% efficiency via perovskite photovoltaics and Earth-abundant catalysts, Science, 345 (2014) 1593-1596.

[53] J. Jia, L.C. Seitz, J.D. Benck, Y. Huo, Y. Chen, J.W.D. Ng, T. Bilir, J.S. Harris, T.F. Jaramillo, Solar water splitting by photovoltaic-electrolysis with a solar-to-hydrogen efficiency over 30%, Nature Communications, 7 (2016) 13237.

[54] A.E. Sanli, A. Aytaç, Response to Disselkamp: Direct peroxide/peroxide fuel cell as a novel type fuel cell, International Journal of Hydrogen Energy, 36 (2011) 869-875.

[55] S. Fukuzumi, Y. Yamada, K.D. Karlin, Hydrogen peroxide as a sustainable energy carrier: Electrocatalytic production of hydrogen peroxide and the fuel cell, Electrochimica Acta, 82 (2012) 493-511.

[56] X.H. Yan, T.S. Zhao, L. An, G. Zhao, L. Shi, A direct methanol–hydrogen peroxide fuel cell with a Prussian Blue cathode, International Journal of Hydrogen Energy, 41 (2016) 5135-5140.

[57] Y. Yamada, Y. Fukunishi, S.-i. Yamazaki, S. Fukuzumi, Hydrogen peroxide as sustainable fuel: electrocatalysts for production with a solar cell and decomposition with a fuel cell, Chemical Communications, 46 (2010) 7334-7336.

[58] S. Fukuzumi, Artificial photosynthesis for production of hydrogen peroxide and its fuel cells, Biochimica et Biophysica Acta (BBA) - Bioenergetics, 1857 (2016) 604-611.

[59] Y. Yamada, M. Yoneda, S. Fukuzumi, High and robust performance of H2O2 fuel cells in the presence of scandium ion, Energy & Environmental Science, 8 (2015) 1698-1701.

[60] J.Y. Kao, C.M. Wang, Electrochemical Study on Decomposition of Hydrogen Peroxide with Fe(II), Journal of the Chinese Chemical Society, 41 (1994) 533-538.

[61] Y. Yamada, S. Yoshida, T. Honda, S. Fukuzumi, Protonated iron-phthalocyanine complex used for cathode material of a hydrogen peroxide fuel cell operated under acidic conditions, Energy & Environmental Science, 4 (2011) 2822-2825.

[62] E.E. Ferapontova, Direct Peroxidase Bioelectrocatalysis on a Variety of Electrode Materials, Electroanalysis, 16 (2004) 1101-1112.

[63] N. Fetner, J.L. Hudson, Oscillations during the electrocatalytic reduction of hydrogen peroxide on a platinum electrode, The Journal of Physical Chemistry, 94 (1990) 6506-6509.

[64] S.A. Mousavi Shaegh, N.-T. Nguyen, S.M. Mousavi Ehteshami, S.H. Chan, A membraneless hydrogen peroxide fuel cell using Prussian Blue as cathode material, Energy & Environmental Science, 5 (2012) 8225-8228.

[65] A. Devadoss, P. Sudhagar, C. Terashima, K. Nakata, A. Fujishima, Photoelectrochemical biosensors: New insights into promising photoelectrodes and signal amplification strategies, Journal of Photochemistry and Photobiology C: Photochemistry Reviews, 24 (2015) 43-63.

[66] L. Han, S. Guo, P. Wang, S. Dong, Light-Driven, Membraneless, Hydrogen Peroxide Based Fuel Cells, Advanced Energy Materials, 5 (2015) 1400424.

[67] A. Devadoss, P. Sudhagar, C. Ravidhas, R. Hishinuma, C. Terashima, K. Nakata, T. Kondo, I. Shitanda, M. Yuasa, A. Fujishima, Simultaneous glucose sensing and biohydrogen evolution from direct photoelectrocatalytic glucose oxidation on robust Cu2O-TiO2 electrodes, Physical Chemistry Chemical Physics, 16 (2014) 21237-21242.

Figure captions

Figure 1. (a) X-ray diffraction results and (b) Texture co-efficient of CZTS films prepared at different processing temperatures.

Figure 2. Raman spectra of CZTS films prepared at different processing temperatures.

Figure 3. SEM image of JNS coated CZTS film prepared at different temperatures (a) 250℃, (b) 300℃ and (c) 350℃ ; and (d) Elemental mapping results recorded at Figure 3a.

Figure 4. The optical absorption (kubelka-munk) results of CZTS films prepared at different temperatures (a) 250℃, (b) 300℃ and (c) 350℃.

Figure 5: Electrical conductivity studies (Log ρ vs 1000/T vs plots) of CZTS films prepared at different temperatures.

Figure 6. Cyclic voltammogram results of CZTS anodes in water oxidation and reduction reaction. The CZTS films were prepared at different temperatures. Aqueous 1 M NaOH is used as electrolyte, scan rate 50 mV/S.

Figure 7. (a) Schematic illustration of electrochemical cells in hydrogen peroxide decomposition and (b) cyclic voltammogram of CZTS cathode in hydrogen peroxide reduction in 0.2 M PBS solution.

Figure 8. (a) Schematic illustration of membrane-free photoelectrochemical cells in hydrogen peroxide reduction into electricity generation; (b) LSV plot of H_2O_2 reduction in dark and light illumination conditions [note that the TiO_2 nanowire is used as photoanode and CZTS is applied as counter electrode]. The H_2O_2 reduction performance using Pt counter electrode, in associate with TiO_2 nanowire and light irradiation is compared in the Figure 8 (dotted line).

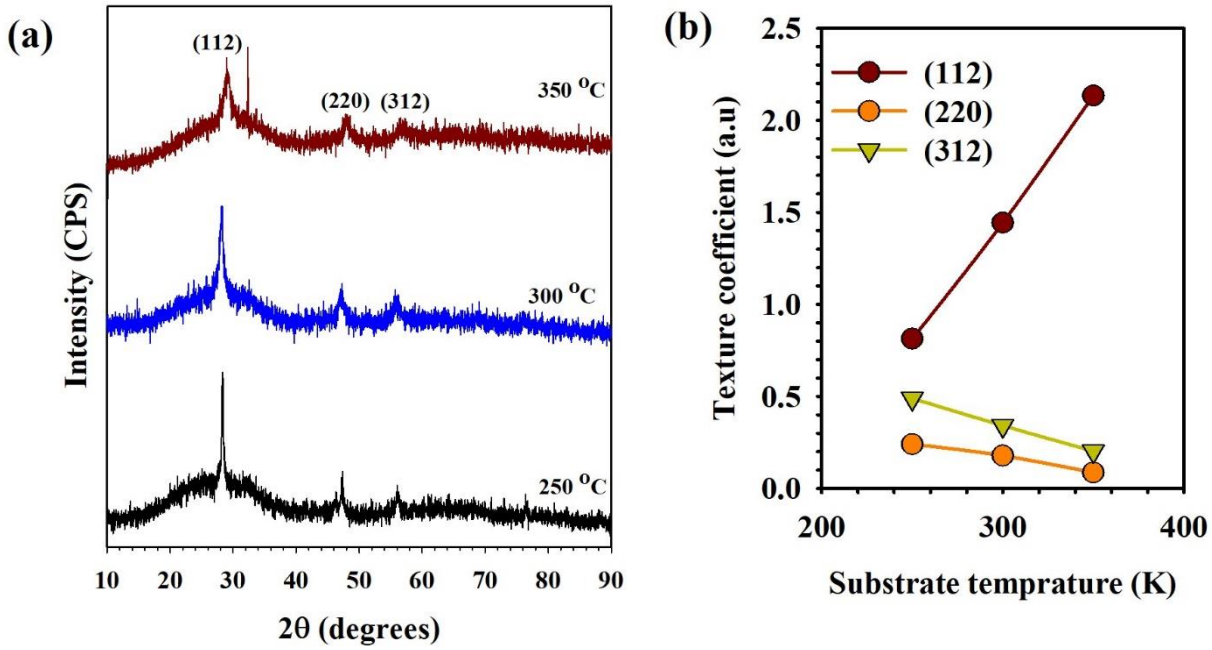
(a)
(112)
(220)
(312)
350 °C
300 °C
250 °C
Intensity (CPS)
10
20
30
40
50
60
70
80
90
2θ (degrees)
(b)
2.5
2.0
1.5
1.0
0.5
0.0
(112)
(220)
(312)
Texture coefficient (a.u)
200
300
400
Substrate temprature (K)

Figure 1

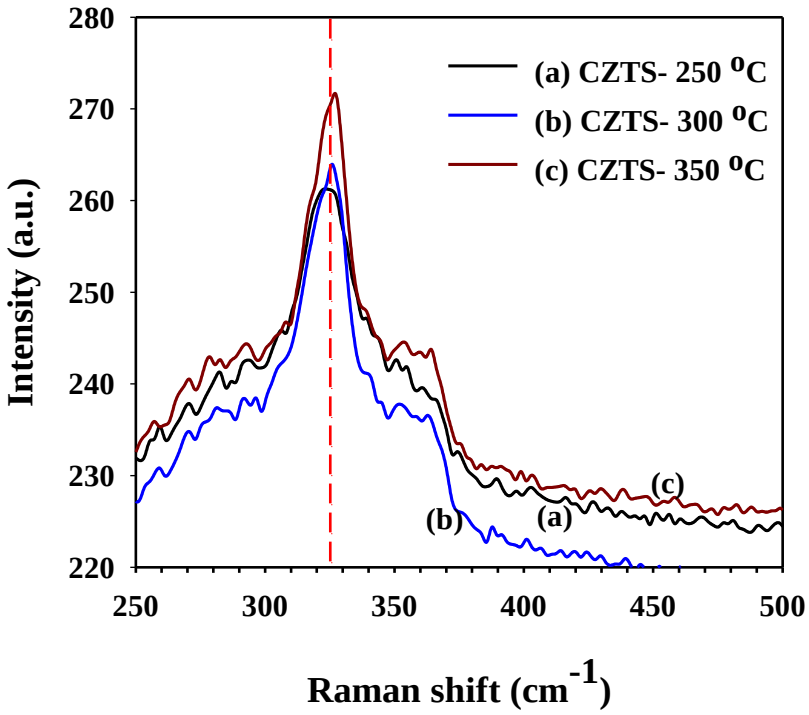
280
270
260
250
240
230
220
Intensity (a.u.)
250
300
350
400
450
500
Raman shift (cm-1)
(a) CZTS- 250 oC
(b) CZTS- 300 oC
(c) CZTS- 350 oC
(c)
(b)
(a)

Figure 2

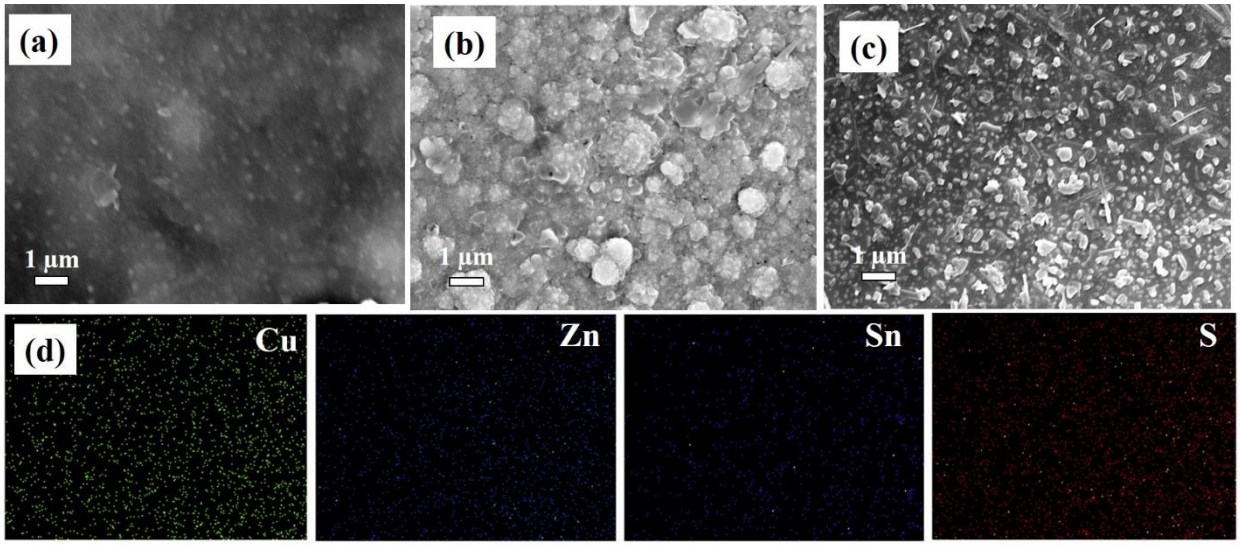

Figure 3

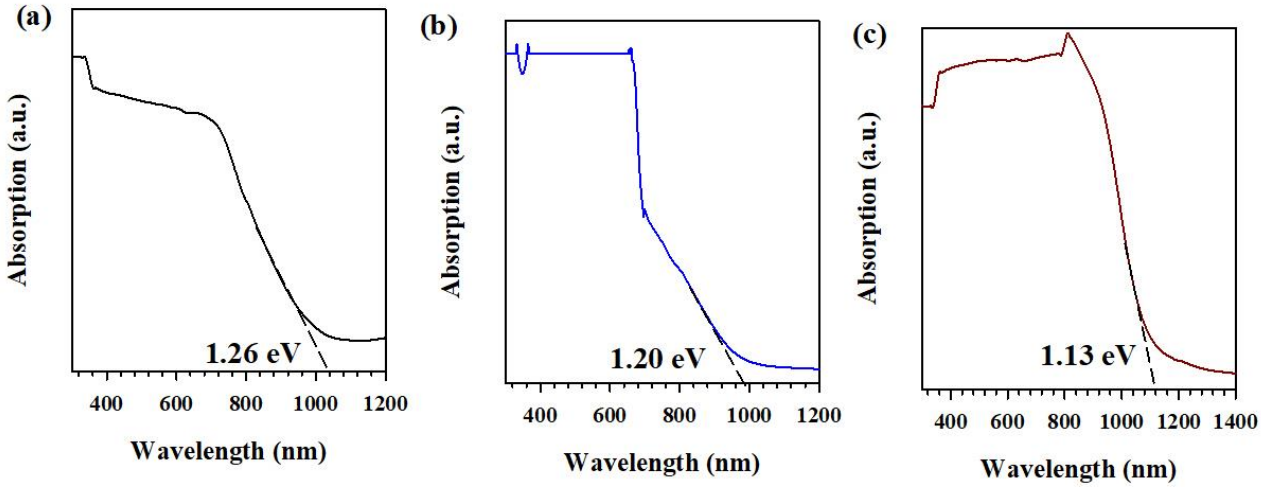
(a)
Absorption (a.u.)
1.26 eV
400
600
800
1000
1200
Wavelength (nm)
(b)
Absorption (a.u.)
1.20 eV
400
600
800
1000
1200
Wavelength (nm)
(c)
Absorption (a.u.)
1.13 eV
400
600
800
1000
1200
1400
Wavelength (nm)

Figure 4

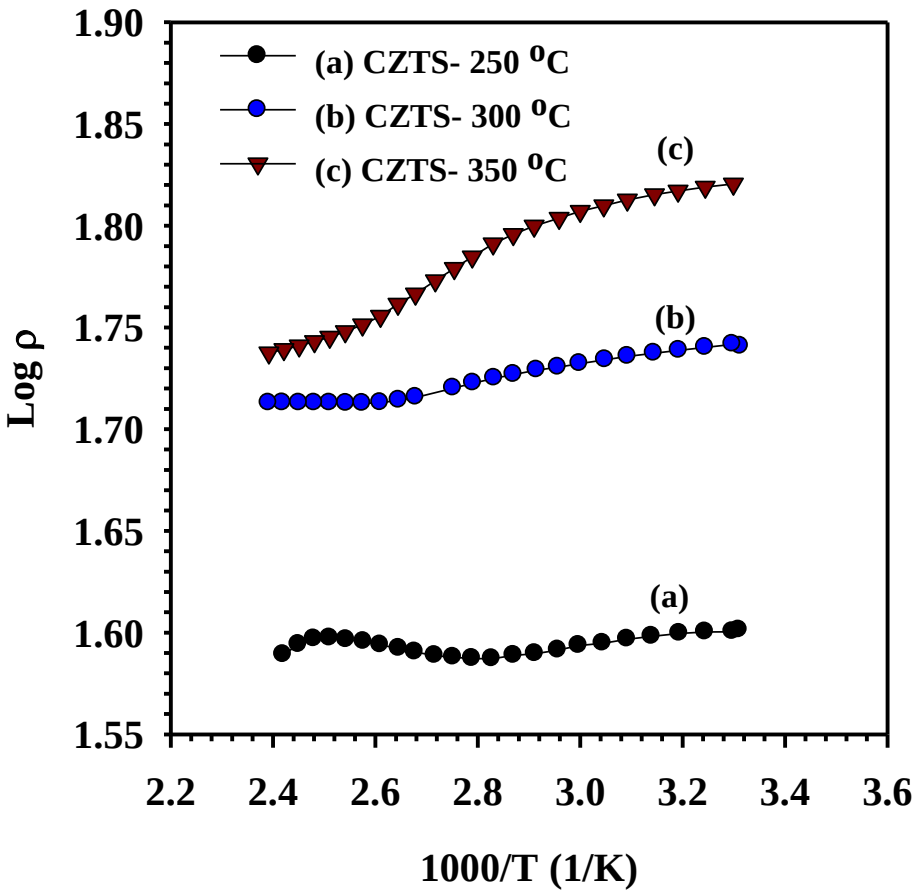
(a) CZTS- 250 °C
(b) CZTS- 300 °C
(c) CZTS- 350 °C
(c)
(b)
(a)
Log ρ
1.90
1.85
1.80
1.75
1.70
1.65
1.60
1.55
2.2
2.4
2.6
2.8
3.0
3.2
3.4
3.6
1000/T (1/K)

Figure 5

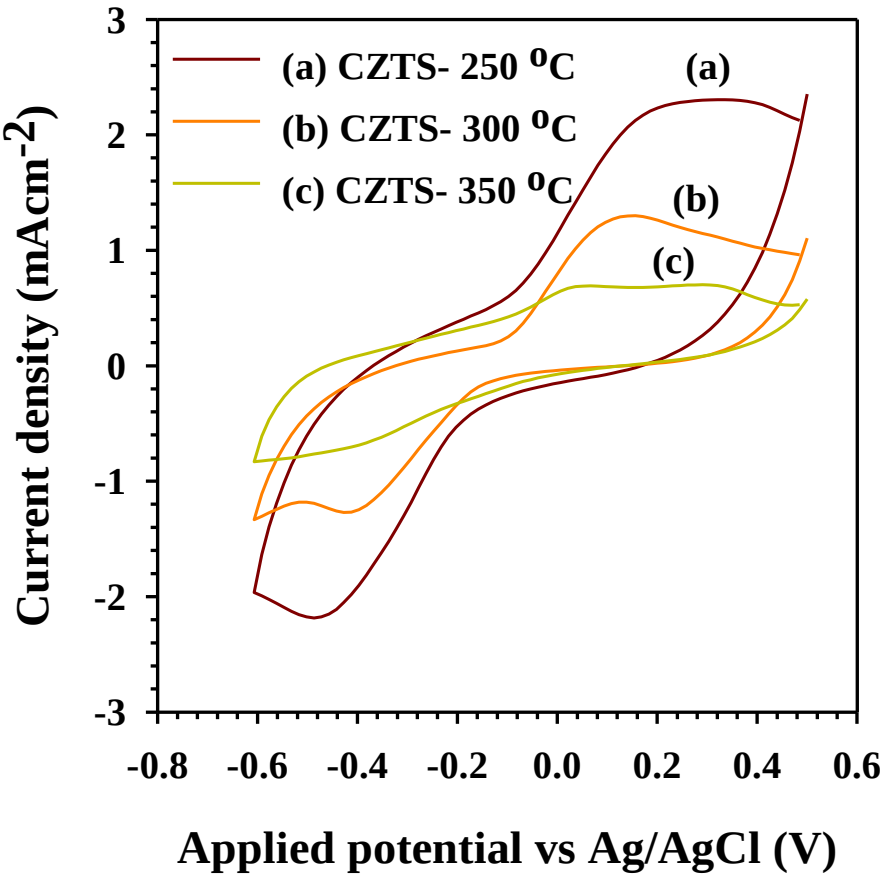
(a) CZTS- 250 °C
(b) CZTS- 300 °C
(c) CZTS- 350 °C
(a)
(b)
(c)
Current density (mAcm-2)
Applied potential vs Ag/AgCl (V)
3
2
1
0
-1
-2
-3
-0.8
-0.6
-0.4
-0.2
0.0
0.2
0.4
0.6

Figure 6

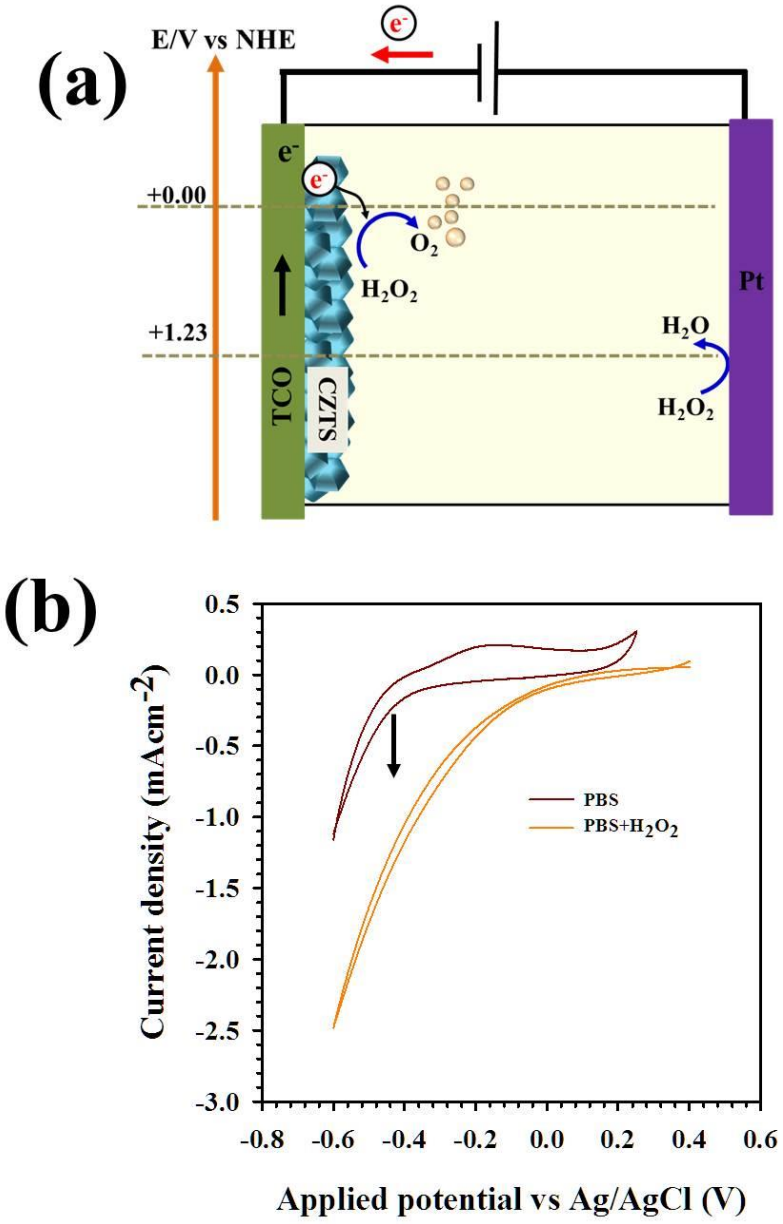
(a)
E/V vs NHE
e-
+0.00
+1.23
O2
H2O2
H2O
H2O2
Pt
TCO
CZTS
(b)
Current density (mAcm-2)
Applied potential vs Ag/AgCl (V)
PBS
PBS+H2O2
0.5
0.0
-0.5
-1.0
-1.5
-2.0
-2.5
-3.0
-0.8
-0.6
-0.4
-0.2
0.0
0.2
0.4
0.6

Figure 7

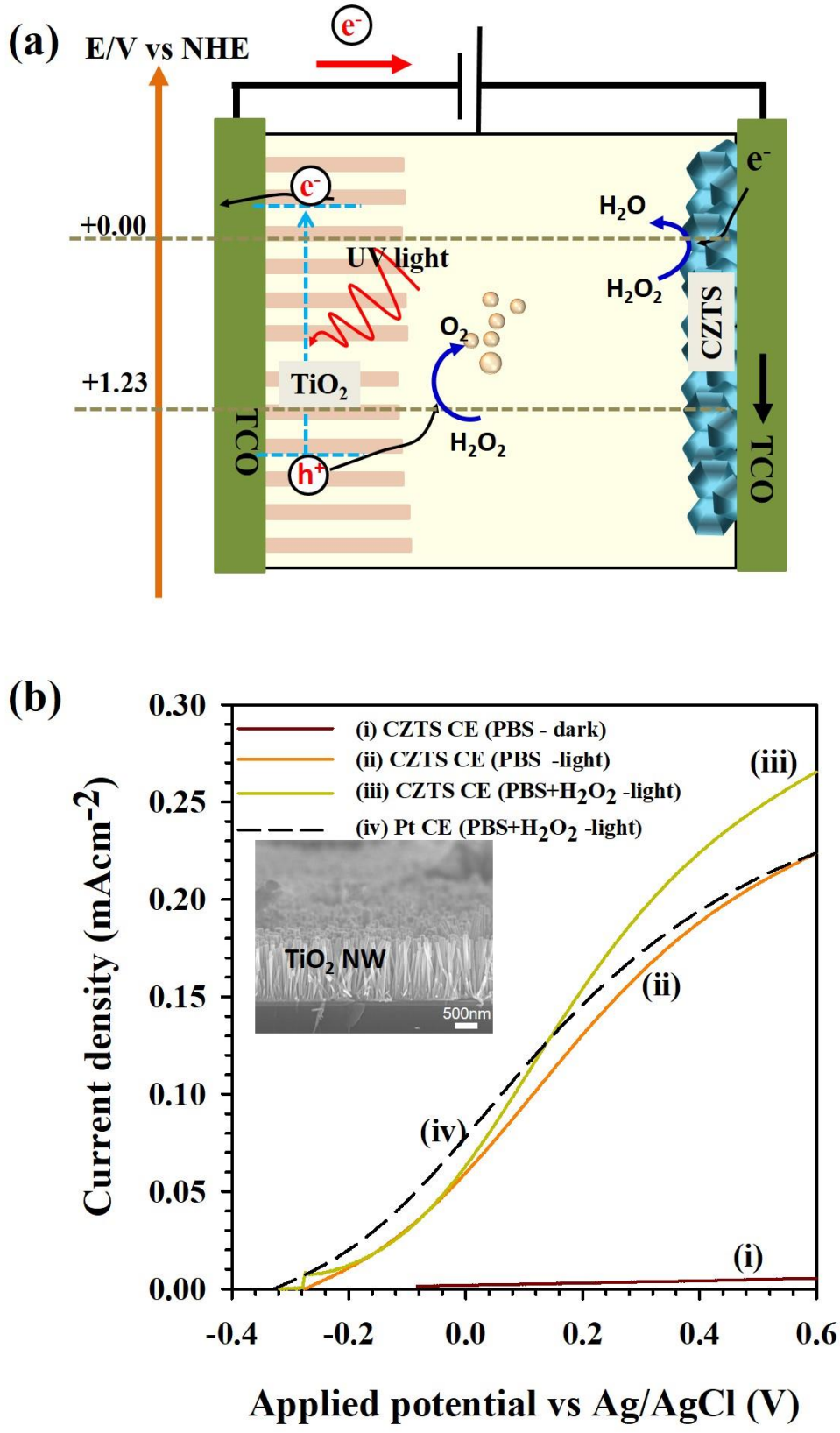
(a)
E/V vs NHE
e⁻
+0.00
+1.23
UV light
TiO2
h+
TCO
O2
H2O2
H2O
CZTS
(b)
(i) CZTS CE (PBS - dark)
(ii) CZTS CE (PBS -light)
(iii) CZTS CE (PBS+H2O2 -light)
(iv) Pt CE (PBS+H2O2 -light)
TiO2 NW
500nm
Current density (mAcm-2)
Applied potential vs Ag/AgCl (V)
0.30
0.25
0.20
0.15
0.10
0.05
0.00
-0.4
-0.2
0.0
0.2
0.4
0.6

Figure 8